An underwater flag-like triboelectric nanogenerator for harvesting ocean current energy under extremely low velocity condition

Yan Wang [a,b], Xiangyu Liu [a], Tianyu Chen [a], Hao Wang [a], Chuanqing Zhu [a], Hongyong Yu [a], Liguo Song [a], Xinxiang Pan [a,c], Jianchun Mi [a,d], Chengkuo Lee [b,*], Minyi Xu [a,*]

[a] *Dalian Key Laboratory of Marine Micro/Nano Enegy and Self-powered Systems, Marine Engineering College, Dalian Maritime University, Dalian 116026, China*
[b] *Center for Intelligent Sensors and MEMS (CISM), National University of Singapore, 4 Engineering Drive 3, 117576, Singapore*
[c] *School of Electronics and Information Technology, Guangdong Ocean University, Zhanjiang 524088, China*
[d] *College of Engineering, Peking University, Beijing 100871, China*

A R T I C L E I N F O

A B S T R A C T

Ocean current energy harvester is a promising infrastructure to achieve self-powered marine wireless sensing system. This study proposes and investigates an underwater flag-like Triboelectric Nanogenerator (UF-TENG) based on the flow-induced vibration. The UF-TENG consists of two conductive ink-coated polyethylene terephthalate membranes and one strip of poly tetra fluoroethylene membrane with their edges sealed up by a waterproof PTFE tape. In this way, the triboelectric layers are prevented from contacting water. It is verified that the vortex street induced by a cylinder enhances the vibration of the UF-TENG. The low velocity startup enables the UF-TENG to harvest extremely low-velocity ocean current energy, e.g., presently achieving 0.133 m/s as the critical startup velocity. The proposed UF-TENG has a simpler structure and better low velocity performance when comparing with electromagnetic generators and piezoelectric generators. Parametric studies are conducted to evaluate the influence of geometrical parameters of the UF-TENG on the vibration behavior and output performance. It is demonstrated that the underwater electrical appliance can be powered by parallel UF-TENG units. The present UF-TENG is a more cost-effective and more accessible hydroelectric technology to utilize the renewable ocean current for powering sensors or micro electric appliances in Internet of Things.

1. Introduction

The ocean energy occurs in various different forms such as wave energy, current energy, thermal gradient energy, etc [1]. The ocean current is a steady directional flow, in contrast to the tidal current along the shore. Ocean currents below and above 100 m deep are usually classified, respectively, as the surface and deep currents [2]; the former is driven primarily by wind. The surface current has a much higher velocity of up to about 300 cm/s, relative to the deep current which moves at less than 10 cm/s [3]. The ocean current has the characteristics of strong regularity, predictable energy density, and relatively stable power generation in different periods. In addition, the ocean current energy harvester does not occupy the land area and does not affect the landscape [4]. The power from ocean currents worldwide was estimated to be over 5000 GW [5]. Although there have been no commercial application cases so far, the ocean current energy is a renewable energy source with a great potential in the future.

Electromagnetic and piezoelectric generators are the most common forms of harvesting the ocean current energy. The electromagnetic generator can effectively harvest ocean current energy, but mainly for the large-scale grid power supply. Electromagnetic generators (EMGs) have been applied for converting ocean current energy into electricity [6,7]. Current EMGs usually have complex hydraulic or mechanical structures to catch ocean current energy. Such designs make the whole device complicated, heavy, and costly [8,9]. More importantly, the EMGs cannot be started at low ocean current velocity. The flow-induced vibration harvester is suitable for harnessing micro-flow energy, such as ocean current energy [10]. Similar to a flag's flapping in the wind, the flapping of a flag-type energy harvester can be also induced by an intrinsic instability of the coupled fluid/body system [11]. In recent years, a piezoelectric generator named Energy Harvesting Eel [12,13] has been proposed to convert hydro-mechanical energy into electricity for powering sensors and robots. The shim stock and electric eels flapped most consistently with the body size of 1.2 m long and 15.25 cm wide at

---

the design flow speed of 1.0 m/s [14]. The flow-induced vibration based piezoelectric generator has a relatively high critical velocity due to the characteristics of piezoelectric material. EMGs and piezoelectric generators do not suit for harvesting the ocean current energy to power a marine wireless sensing system under low flow velocity conditions.

Recently, triboelectric nanogenerator (TENG) has been invented, which has comprehensive applications in the various types of mechanical energy harvesting (wind energy [15–21], wave energy [22–30], vibration energy [31–36], sliding energy [37–39] and acoustic energy [40,41], etc.) and high sensitive self-powered sensing systems [42–46]. Numerous triboelectric nanogenerators have been developed to harvest blue energy, especially at low frequencies (i.e., below 5 Hz). Kim et al. [47] demonstrated a floating buoy-based triboelectric nanogenerator (FB-TENG) that can harvest wave energy effectively in a wild sea state. The electrical appliance can be powered by the FB-TENG in small amplitude waves. Xi et al. [48] designed a multifunctional TENG for scavenging blue energy. Their multifunctional TENG consisted of rotation TENG (r-TENG) and cylindrical TENG (c-TENG). Water flow energy can be harvested by r-TENG, while the water wave energy can be harvested by c-TENG. Commercial LEDs were lightened to demonstrate its outstanding performance. Xu et al. [49] proposed a coupled TENG networks to efficiently harvest water wave energy. The network, based on optimized ball-shell structured TENG units, provides an effective approach toward massive harvesting of water wave energy in the ocean. A plenty of research has focused on wave energy harvesting. However, research on ocean current energy harvesting has not been systematically conducted. Most of the reported water current energy harvesting TENGs aim for usage on the surface of the water [50,51]. They can hardly harvest underwater ocean current energy as their tribo-layer structure is exposed in water. Meanwhile, no previous work has not studied the influence of flow velocity on power generation performance, which turns out to be a very important parameter of the ocean current. The TENG with inspirations from a flapping flag can be used to effectively harvest wind energy. Zhao et al. [52] proposed a flag-type TENG to harvest high-altitude wind energy. A flag-type hybrid wind energy harvester based on triboelectric and electromagnetic was invented by Ye et al. [53]. They showed that the flow-induced vibration on a TENG can be used to effectively harvest flow energy. More importantly, a novel humidity resisting flag-type TENG for harvesting wind energy was developed by Wang et al. [54]. They conducted parametric studies to evaluate the influence of geometrical parameters of the flag-type TENG on the flutter behavior and the resulting energy output. Their demonstration experiments proved that a flag-type TENG can harvest ambient low-speed wind or airflow energy under high humidity natural conditions. Hence, the flag-type TENG is expected to act as an effective way to harvest ocean current energy.

The present study is designated to verify this expectation. First, it proposes the following design for a flexible underwater flag-like TENG (UF-TENG) system for harvesting ocean current energy. This system includes a cylindrical structure that installs upstream of the UF-TENG. The present underwater flag-like triboelectric nanogenerator has a simpler structure and better low-velocity performance compared with electromagnetic generators and piezoelectric generators. It is anticipated that the vortex street induced by the cylinder enhances the vibration of the UF-TENG, thus significantly improving the electrical output at lower flow velocities. Secondly, we study the dynamics of the UF-TENG immersed in flowing water. The effects of various parameters including the aspect ratio and the bending stiffness on the critical velocity and the electrical output performance of the UF-TENG are systematically investigated so as to determine its optimal structural parameters. The proposed UF-TENG provides a feasible and cost-effective way to harvest extremely low velocity ocean current energy and power the marine sensing system.

2. 2. Results and discussion

2.1. Structure and working principle of the UF-TENG

Obviously, flags can flap in the wind. Likewise, similar structures can also vibrate under water flow excitation. This phenomenon has inspired us to develop a UF-TENG which can be driven by the ocean current, see Fig. 1a. Combining the flow-induced vibration with the TENG is a feasible way to convert the mechanical energy to electricity [55–58]. As shown in Fig. 1b, the designed UF-TENG is installed in the flowing water to harvest water flow energy. As shown in the Fig. 1c, the UF-TENG is made of two conductive ink-coated polyethylene terephthalate (PET) and one strip of PTFE membrane pasted together by the PTFE waterproof tape.

Contacting surface schematic of the UF-TENG is shown in Fig. 2a. There is an air gap between the conductive ink-coated PET film and PTFE film due to the separation of adhesive tape. The air gap and microstructure ensure that the UF-TENG can maintain a stable output performance even underwater. Both of the conductive ink-coated PET film surface and PTFE film surface are polished with the 10,000-mesh sandpaper. Fig. 2b and c show the micro-structure on the ink-coated PET film and the PTEF film.

The working principle is demonstrated in Fig. 2d. The materials used in the UF-TENG have different bending modulus. Consequently, the corresponding deformation of materials in the vibration process becomes different. The working mechanism is based on the contact separation model in which three major steps are involved. In the first step, the PTFE membrane and flexible electrode are separated as the adhesive tape exists. The same amounts of charges are generated on the PTFE and the flexible electrode, respectively, as a result of electrostatic induction, see Fig. 2d(i). The UF-TENG starts to vibrate when it is excited by the ocean current, while PTFE contacts with the flexible electrode. When the PTFE membrane comes into contact with the lower electrode, all the positive charges flow to this electrode, so that a transient current is generated in the external circuit, see Fig. 2d(ii). Subsequently, the reversed flapping of the PTFE membrane leads to a reversed transfer of electrons through the external circuit (Fig. 2d(iii)). The commercial software of COMSOL Multiphysics is employed to calculate the electrostatic field distribution of the TENG. The results are shown in Fig. 2e. Apparently, the simulation results are consistent with the above analysis.

According to the theory of the contact-mode freestanding TENG, the output voltage (V) equation for the TENG can be written as [59]:

$$V = -\frac{1}{C}Q + V_{OC} = -\frac{d_0 + g}{\varepsilon_0 S}Q + \frac{2\sigma x}{\varepsilon_0} \tag{1}$$

In Eq. (1), Q is the total transferred charge, V_{OC} is the open circuit voltage, while C, d_0, g, ε_0 and S represent the capacitance of the TENG, the thickness of the membrane, the distance between two electrodes, the dielectric constant in vacuum and the area of the electrode, respectively; x denotes the displacement between the PTFE membrane and the electrode, and σ is the charge density.

2.2. The flow-induced vibration of the UF-TENG

The vibration of a flag-type structure is induced by the intrinsic instability of the coupled fluid/body system. According to the theoretical derivation of Shelley et al. [11] and Zhu et al. [60], a necessary condition for this kind of instability is that the structure has a large inertia. Increasing the mass of the flag-type structure in a limited range can enhance vibration amplitude. Considering that the flow velocity of the ocean current is normally low, the efficiency of the flag-type energy harvester is unsatisfactory at low flow velocity condition. An effective method to improve its performance is to place the flag-type energy harvester (or "eel") in the near wake of a bluff body as shown in Fig. 3a. In this way, the vortex forming behind the bluff body can enhance the
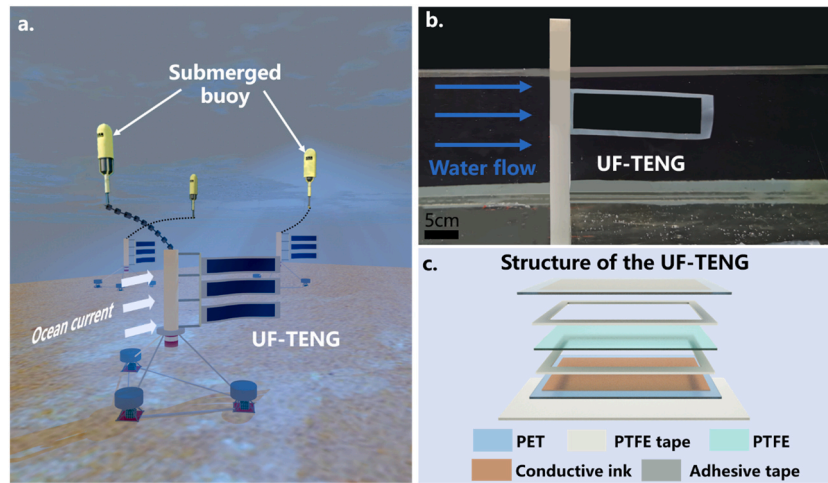
Fig. 1. Structure of the UF-TENG. (a) Prototypes of the UF-TENG and self-powered submerged buoys; (b) UF-TENG in flowing water; (c) detailed structure of the UF-TENG.
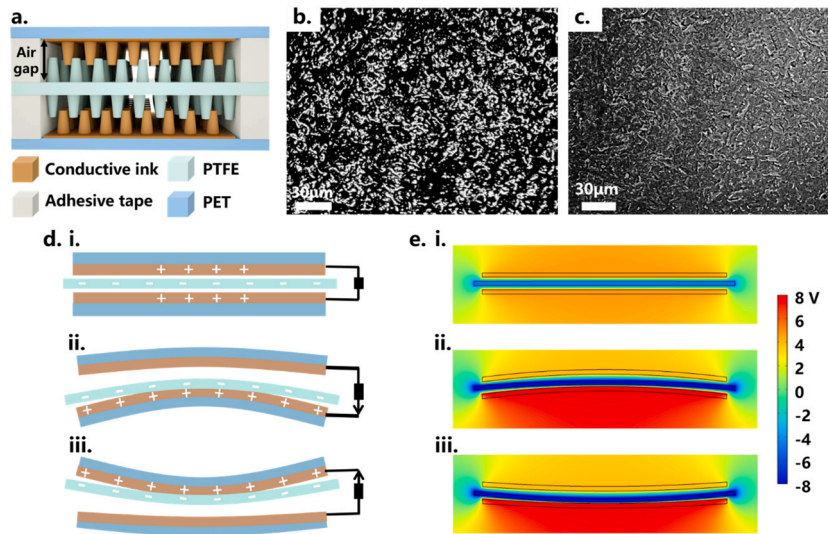
Fig. 2. (a) Schematic illustration of the contacting surface; SEM micrograph of (b) the PTFE film surface; (c) the conductive ink-coated PET film surface; (d) working principle of the UF-TENG; (e) finite element simulation of the UF-TENG.

vibration of the harvester [12,13]. As shown in Fig. 3a and b, the flexible UF-TENG with dimension of 140×35 mm^2 is installed on a supporting frame and placed in a circulating water flume. At the flow velocity of 0.228 m/s, the non-vibration and vibration states of the UF-TENG are shown in Fig. 3c and d, respectively. The vibration amplitude is greatly enhanced by the vortex shedding and traveling while the critical velocity is decreased.

Numerous studies investigated the flapping stability and response of a thin two-dimensional flag or cantilevered flexible plates in uniform flow [17,61–65]. The ratio of the fluid mass to flag mass M^* defined below:

$$M^* = \frac{\rho_f L}{\rho_s h} \tag{2}$$

is the important nondimensional parameter that determines the critical flow velocity of the flag. In Eq. (2), L is the length of the flag, ρ_f is the density of the fluid, ρ_s is the density of the flag, h is the thickness of the flag. The work of Shelly et al. [11] emphasized the importance of flag inertia in overcoming the stabilizing effects of finite rigidity and water drag. By increasing the mass of the flag, the critical flow velocity

decreased sharply. However, larger mass results in higher critical velocity of the flag-type structure in wind. This is the difference between the vibration of the flag in water and air.

For the UF-TENG to achieve larger amplitude vibration at low flow velocity, placing a cylinder upstream of the flag-like energy harvester is a common method. Allen and Smits [12] placed an energy harvesting eel in the wake of a bluff body to use the von Karman vortex street forming behind the bluff body to induce oscillations in the membrane. The vibration of the UF-TENG can be demonstrated with a superposition of the free (f_1) and forced (f_2) vibrations [12], which is governed by the following equation:

$$m\ddot{y}(t,x) + H(\dot{y}, \quad y, \quad x, \quad t) = f_1 + f_2 \quad . \tag{3}$$

here, $y(x, \quad t)$ is the displacement of the structure in the spanwise direction, m is the mass of the structure, H represents internal restoring forces related to the body stiffness and damping properties. The corresponding coordinate system is shown in Fig. S2. The term f_1 is the free vibration which can be expressed as the Movement Induced Excitation (MIE) [66]. Kim et al. [67] revealed that a flexible foil can sustain large amplitude oscillations under low critical wind speed. In their work, the
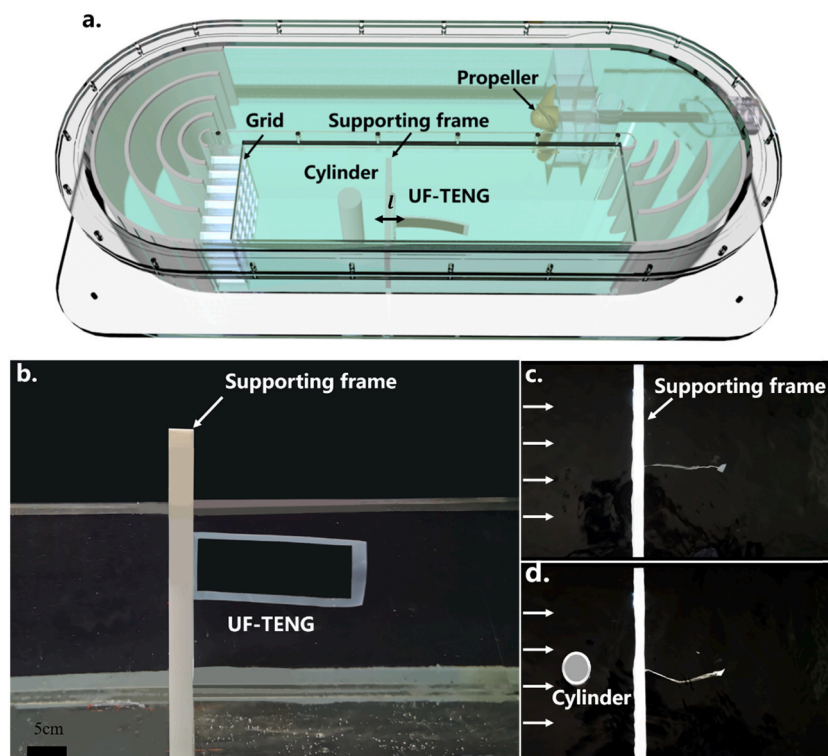
Fig. 3. Experimental setup of the UF-TENG. (a) Schematic of the experimental setup; (b) UF-TENG in flowing water; (c) the none-vibration state, and (d) the vibration state induced by the cylinder vortices at the flow velocity of 0.228 m/s.

non-dimensional bending stiffness (K_B) defined below:

$$K_B = \frac{Eh^3}{12(1-\nu^2)\rho_f U^2 L^3} \tag{4}$$

(where h is the thickness of the UF-TENG, E the Young's modulus and U the flow velocity, ν the Poisson's ratio) is considered critical for the study of interaction between a fluid flow and an elastic sheet. The MIE is mainly caused by the force of the fluid acting on the elastic sheet.

Moreover, the term f_2 in Eq. (3) denotes the effect of an external force induced by the Karman vortex, which can be expressed as Extraneously Induced Excitation (EIE). Allen and Smits [12] studied the enhancement of the bluff-body vortex shedding on the membrane oscillation, experimentally showing that the vortex street forming behind a bluff body induces the oscillation.

Present experiments on the parameter sensitivities for the UF-TENG are performed in a circulating water flume. Parameters of the flag in this work are listed in Table S1. A high-speed camera is used to record the vibration trails. Fig. 4a and Supplementary movie 1 shows the vibration and enhanced vibration of the UF-TENG when $M^* = 1270$ and $L/W = 4$. When the UF-TENG is tested in the water current of 0.156 m/s, the vibration amplitude is very low (the UF-TENG almost keeps stable), as shown in Fig. 4a(i). After a cylinder with $D = 35$ mm diameter is installed upstream of the UF-TENG, the vibration amplitude is greatly enhanced by the Karman vortices shedding from the cylinder, as shown in Fig. 4a(ii). Also, the amplitude of the UF-TENG increases as the flow velocity rises, see Fig. 4a(iii). Fig. 4b shows the critical velocity (U_c) versus the UF-TENG's length (L) and aspect ratio (L/W) when the cylinder is installed upstream of the UF-TENG. Increasing L (then the flag mass) results in a lower U_c, which agrees well with the prediction of Argentina and Mahadevan [73] on the critical speed of a flag. Besides, a decrease in L/W due to increasing W (also the flag mass) leads to a lower critical velocity as a lower L/W results to a higher mass (or higher inertia) of the flag. This somehow coincides with Shelley et al. [11] who found a lower critical velocity under a higher inertia of flag in water.

Note that the magnitude of V_{oc} is associated to the fluid–solid mass ratio M^* as shown in Fig. 4c and d, which means that an increase of the mass ratio leads to an increase of the open circuit voltage at the flow velocity of 0.223 m/s. As the lower L/W means a large area of the flag, thus it could lead to a high output voltage with the same M^*. This result can be obtained from Eq. (1) that higher S can result in a high output voltage. As depicted in Fig. 4a(ii) and a(iii), the amplitude of the UF-TENG increases as the flow velocity rises. Larger amplitude leads to a larger S, thus the output voltage at a flow velocity of 0.461 m/s is higher than that of 0.223 m/s as shown in Fig. 4d. As shown in Fig. 4e, when the distance between the UF-TENG and the cylinder is within the range of $1D \sim 5D$, the critical velocity stays almost unchanged. However, when the distance is increased beyond $6D$, the critical velocity increases sharply by 68%. This indicates that the enhancement of the vortex street depends on the Karman vortex strength, which decays with downstream distance. When the distance exceeds $6D$, the enhancement has disappeared, or the vortex street has no effect on the vibration of the UF-TENG.

Supplementary material related to this article can be found online at doi:10.1016/j.nanoen.2021.106503.

The present UF-TENG appears to have overcome the problem of various existing ocean current harvesters that cannot work well under low-velocity current conditions. Despite a huge potential of ocean currents, a practical challenge in harvesting the current energy is how to reduce the critical velocity of energy harvesters. The experimental data [13,68–72,74] concerning output performances of electromagnetic generators, piezoelectric generators and triboelectric nanogenerators are presented in Table S2 for comparison, which includes ocean current energy harvesters with good output performance for each method. Fig. 4f depicts the critical velocity comparison. The present UF-TENG has the lowest critical velocity, which implies its application potential under low-velocity conditions. The enhancing effect occurs when the UF-TENG is placed in the vortex street. Here we have used the cylinder diameter (D) as the characteristic length of the system, and examined the critical velocity of the UF-TENG.
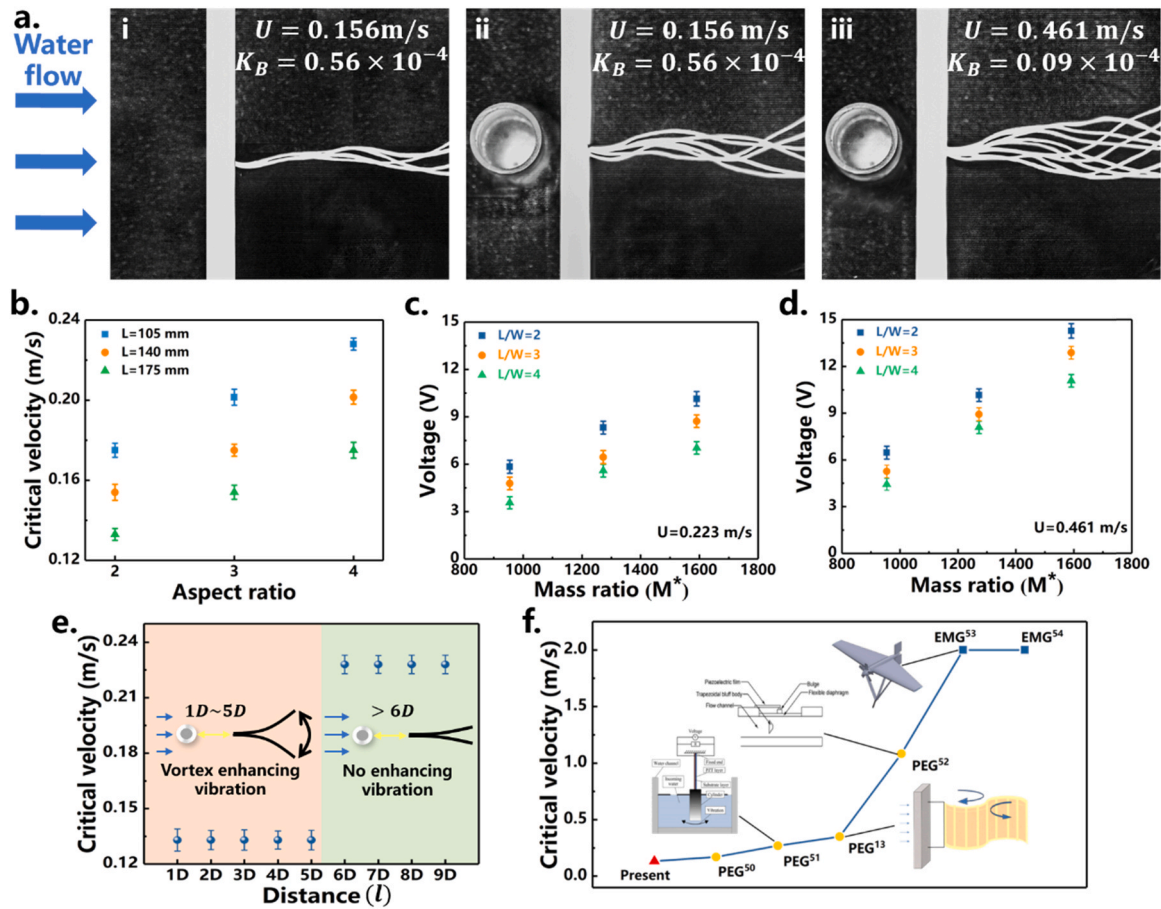
Fig. 4. Vibration characteristic of the UF-TENG. (a) The vibration dynamics comparison between the UF-TENG and vortex enhanced UF-TENG; (b) effect of the aspect ratio on the critical flow velocity; dependence of the open circuit voltage on mass ratio with (c) flow velocity 0.223 m/s; (d) flow velocity 0.461 m/s; (e) dependence of the critical velocity on the distance between the UF-TENG and the cylinder; (g) the present starting velocity versus those previously of, piezo-flag [68], VIPEH [69], EEL [13], pressure fluctuation piezoelectric energy harvester [70], TUSK [71] and MHK [72].

2.3. Electrical output performance of the UF-TENG

In the water flume experiments, the vortex enhancing effect on the vibration of the UF-TENG has been verified. Fig. 5a shows the schematic diagram of the UF-TENG's working state while Fig. 5b compares the voltage signals of the two UF-TENG ($L = 140$ mm, $L/W = 4$) with $M^* = 1270$. Evidently, at the flow velocity of 0.461 m/s, the existence of a cylinder increases the output performance substantially by 170%. It follows that the output voltage, current, and transferred charge all rise greatly, as seen in Fig. 5c. The open circuit voltages of the UF-TENG are presented in Fig. 5d–f as a function of the flow velocity (U) or the bending stiffness (K_B). Note that $K_B \sim U^{-2}$, see Eq. (4). A higher output voltage is produced by the UF-TENG at a lower bending stiffness and/or an aspect ratio. The output voltage of 14.4 V is obtained at $U = 0.461$ m/s (or $K_B = 0.06 \times 10^{-4}$) when $M^* = 1590$ and $L/W = 2$ in the circulating water flume. Higher output voltage can be observed at higher mass ratio as shown in Fig. 5d–f. The critical velocity for the vibration is determined by the mass ratio as shown in Fig. 5d–i. Lower critical velocity and higher output performance can be obtained by increasing the mass ratio from 955 to1590. An output voltage of about 12.8 V and output current of about 0.81 µA is achieved at a low critical velocity of 0.133 m/s with a flag mass ratio of 1590, as shown in Fig. 5f and i. Higher flow velocity results in larger vibration amplitude according to Fig. 4a. Larger contact area of the triboelectric layer can be obtained by larger vibration amplitude. The small voltage slope may be due to the small increase rate of the contact area with the flow velocity. The output current of the UF-TENG continues to rise with the flow

velocity, and the slope is larger than that of voltage. Shelley et al. [11] showed that the vibration frequency of a flag is proportional to the flow speed. The vibration frequency of the UF-TENG is also increased by increasing the flow velocity, which results to an increasing of the output current as shown in Fig. 5g–i. Output current of 1.43 µA can be reached when the flow velocity increases from 0.133 m/s to 0.461 m/s as shown in Fig. 5i.

There have been many studies on the vibration mode of the flag-like structure which depends on the flow velocity [75–77]. High flow velocities result in multi-ordered vibration modes. There are multiple vibration crests in the multi-ordered mode. The triboelectric electrons generated by the opposite crests cancel out each other, thus reducing the electric output of the TENG. The designed UF-TENG is mainly for the extremely low velocity conditions. Physical dimensions for the experimental samples are listed in Table S3. In the tested flow velocities (0.133–0.461 m/s), the vibration of the UF-TENG is stable or of the 1st mode. Besides, the flag-like TENG can tune itself with the flow direction, which can be considered as another advantage of the UF-TENG. The ocean current is a steady directional flow. Once there is a slight change in the flow direction, the UF-TENG can tune itself in that direction. The UF-TENG can keep a constant output performance in theory.

According to Eq. (1), the distance between the two electrodes (g) is one of the key parameters that determine the performance of the UF-TENG. Increasing the thickness of the flag-type TENG (d_0) results in the increase of the bending stiffness of the TENG. The critical speed increases dramatically with the increment in g. It is not appropriate to enhance the output performance by increasing g. The similar results
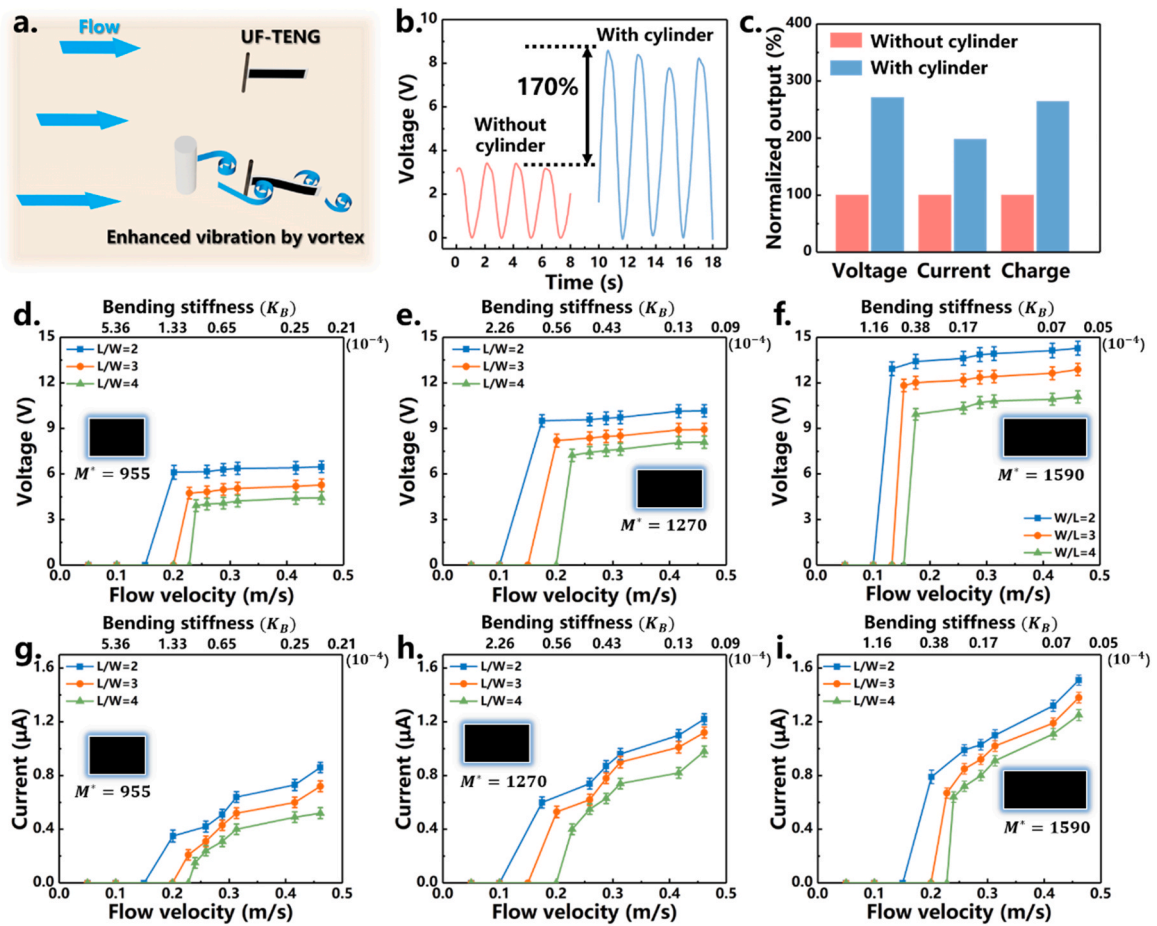
Fig. 5. Output performance comparison and voltage, current vs. flow velocity and bending stiffness (not to scale) for different aspect ratios (L/W) of the UF-TENG. (a) Schematic of the UF-TENG working state; (b) output voltage signal comparison of the UF-TENG with $M^* = 1270$; (c) comparison in the output performance between the UF-TENGs with and without cylinder; open circuit voltages of the UF-TENG at different aspect ratios and bending stiffnesses with (d) $L = 105$ mm, (e) 140 mm and (f) 175 mm; short circuit currents of the UF-TENG with (g) $L = 105$ mm, (h) 140 mm and (i) 175 mm.
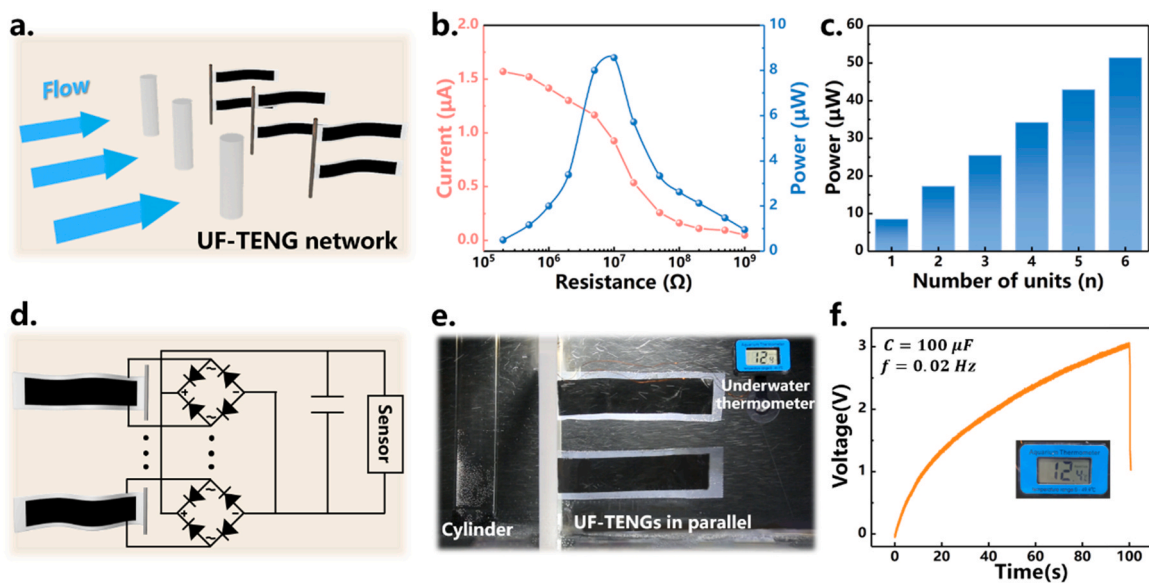

Fig. 6. Integrated UF-TENG unit array. (a) Schematic of the six UF-TENG units; (b) dependence of the output current and power on the external resistance for the UF-TENG; (c) the output power when working under different unit of the UF-TENG; (d) schematic diagram of six UF-TENG units and working circuit to power sensor; (e) the photograph an underwater thermometer powered by six UF-TENG units; (f) powering an underwater thermometer with six UF-TENG units.

have been achieved from the UF-TENG. As shown in Fig. S3, increasing *g* from 0.11 mm to 0.23 mm, the critical velocity of the UF-TENG increases greatly. In addition, the output voltage and current reduction as the contact area and/or the vibrating frequency decrease.

The durability test is conducted to show the robustness of the UF-TENG. As shown in Fig. S4, the output voltage is steady over 3000 s at the flow velocity of 0.175 m/s, and the device output voltage is consistent over 300 s in 3 days, implying that the device is durable.

2.4. Integrated UF-TENG array

The demonstration experiments are conducted to illustrate the application of the UF-TENG. The electrical output performance can be improved by connecting manifold UF-TENG units in parallel. The schematic diagram of six UF-TENG units is presented in Fig. 6**a**. The peak output power of a UF-TENG can reach 9.1 μW under a loading resistance of 10 MΩ, see Fig. 6**b**. Fig. 6**c** shows the total output power of the UF-TENG (P_N) versus the number of the UF-TENG units (N). Manifestly, the total output power grows almost linearly with the unit number, i.e., $P_N = NP_1$. For example, the total output power of 6 UF-TENG units is six times that of one UF-TENG unit as *N* is increased from one to six. The structure diagram of the integrated devices composed of 6 UF-TENG units and the corresponding circuit is presented in Fig. 6**d**. As can be seen in Fig. 6**e**, an underwater thermometer is powered by six UF-TENG units. The video of powering an underwater thermometer is shown in Supplementary movie 2. Fig. 6**f** demonstrates that the underwater thermometer has been successfully activated after charging the 100 μF capacitor for 100 s. Some commonly used sensors in ocean monitoring systems are shown in the Fig. S5. By implementing sufficient number of UF-TENG units, various sensors can be driven. As can be observed from the figure, the proposed UF-TENG is more suitable for harvesting extremely low-velocity ocean current energy and powering distributed sensor nodes with its simple structure, low-cost and better low-velocity outputs.

Supplementary material related to this article can be found online at doi:10.1016/j.nanoen.2021.106503.

3. Conclusion

Most ocean-current-power applications are limited to a relatively high starting ocean current velocity. An ocean current energy harvester with a lower velocity startup and a wider working range is desperately needed. To address this need, we have developed and studied a flexible underwater flag-like TENG for harvesting ocean current energy. In particular, the present UF-TENG can work through its vibration induced by the ocean current. In order to further improve the output performance of the UF-TENG, a cylindrical structure is adopted to induce the Karman vortex street, which proves to greatly enhance the vibration of the UF-TENG. The vortex street enhanced UF-TENG vibration is evident by the envelope captured by high-speed camera, the critical velocities measured under various cylinder distances are the evidence of vortex street enhancing UF-TENG vibration. The enhanced vibration UF-TENG turns out to be capable of harvesting ocean current energy at a low current speed. The UF-TENG can be induced to vibrate by a water flow with the velocity ≥ 0.0133 m/s via adjusting its bending stiffness ($K_B \leq 0.65 \times 10^{-4}$). Meanwhile, by conducting experiments in a circulating water flume, the UF-TENG with the mass ratio of 1590 demonstrates a higher output performance. A peak output power of 52.3 μW can be achieved with six UF-TENG units at the flow velocity of 0.461 m/s. Compared with the PEG/EMG, the UF-TENG yields a lower critical velocity, which is a significant advantage in harvesting low-velocity ocean currents. This study contains systematic experimental fluid dynamics studies, which is a quite meaningful addition to the endeavor of harvesting ocean kinetic energy with TENG. However, the effect of high pressure under deep water condition on the output performance remains open to explore. A UF-TENG that can work in deep water is to be developed in the future.

4. Experimental section

4.1. Manufacture of the UF-TENG

The fabrication of the UF-TENG is shown in Fig. 1**c**. The thickness of the PTFE, PET membranes, the waterproof PTFE tape and the adhesive tape is 50 μm, 25 μm, 30 μm and 30 μm, respectively. A conductive ink electrode with a micrometer thickness was attached to the back side of the PET as the flexible electrode. The conductive ink (#CH-8(MOD2) from JUJO printing supplies & technology (Pinghu) Co. Ltd) is printed on the FEP and PET membrane by the screen-printing technology. Then, it dries under the atmospheric temperature. Fig. 1**c** demonstrates that the dimension of the lower flexible electrode is smaller than the PTFE, while the upper flexible electrode is larger than PTFE. The waterproof PTEF tape has the largest dimension when comparing to the PTFE membrane and two flexible electrodes. The PTFE tape and the upper flexible electrode are pasted together by the adhesiveness of the PTFE tape itself, so that the triboelectric layers can be sealed by the PTFE tape. The UF-TENG and the flagpole are connected together by the sticky tape. The integrated device is installed in a PLA supporting frame as shown in Fig. 3**a**. When water current flows along the UF-TENG, it can vibrate periodically, thereby producing alternating voltage and current signals. By installing a cylinder upstream of the UF-TENG, the vibration effect and power generation performance of the UF-TENG can be improved.

4.2. Electrical output measurement

The experiments for the UF-TENG are performed in a circulating water flume with a test section of 0.25 m (width) × 0.25 m (height) × 0.9 m (length). The water current velocity varies from 0.133 m/s to 0.511 m/s. A propeller is used to generate water current, and an inverter is used to control the rotating speed of the propeller. The detailed envelope is captured by the high-speed camera (FATCAM Mini UX50). A flow meter is placed at the test domain to calibrate the water current velocity. To measure the electrical output of the UF-TENG, a programmable electrometer (Keithley Model 6514) is used.

CRediT authorship contribution statement

Yan Wang: Conceptualization, Methodology, Writing – original draft. **Xiangyu Liu:** Formal analysis, Data curation. **Tianyu Chen:** Software, Formal analysis. **Hao Wang:** Validation. **Chuanqing Zhu:** Fabricated and assembled the UF-TENG. **Hongyong Yu:** Performing experiments. **Liguo Song:** Performing demonstration experiments. **Xinxiang Pan:** Funding acquisition. **Jianchun Mi:** Writing – review & editing. **Chengkuo Lee:** Writing – review & editing. **Minyi Xu:** Supervision, Writing – review & editing.

Declaration of Competing Interest

The authors declare that they have no known competing financial interests or personal relationships that could have appeared to influence the work reported in this paper.

Acknowledgments

Appendix A. Supplementary material

Supplementary data associated with this article can be found in the online version at doi:10.1016/j.nanoen.2021.106503.

References

[1] A.S. Bahaj, Generating electricity from the oceans, Renew. Sustain. Energy Rev. 15 (2011) 3399–3416, https://doi.org/10.1016/j.rser.2011.04.032.

[2] H. Stommel, A survey of ocean current theory, Deep Sea Res. 4 (1957) 149–184, https://doi.org/10.1016/0146-6313(56)90048-X.

[3] G. Shanmugam, Gravity Flows, and Bottom Currents: Downslope and Alongslope Processes and Deposits, Elsevier, 2020.

[4] A.S. Bahaj, L.E. Myers, Fundamentals applicable to the utilisation of marine current turbines for energy production, Renew. Energy 28 (2003) 2205–2211, https://doi.org/10.1016/S0960-1481(03)00103-4.

[5] Ocean Current Energy Potential on the U.S. Outer Continental Shelf, Minerals Management Service Renewable Energy and Alternate Use Program, U.S. Department of the Interior, 2006.

[6] M. Melikoglu, Current status and future of ocean energy sources: a global review, Ocean Eng. 148 (2018) 563–573, https://doi.org/10.1016/j.oceaneng.2017.11.045.

[7] A. Westwood, Ocean power: wave and tidal energy review, Refocus 5 (2004) 50–55, https://doi.org/10.1016/S1471-0846(04)00226-4.

[8] S.L. Zhang, M. Xu, C. Zhang, Y. Wang, H. Zou, X. He, Z. Wang, Z.L. Wang, Rationally designed sea snake structure based triboelectric nanogenerators for effectively and efficiently harvesting ocean wave energy with minimized water screening effect, Nano Energy 48 (2018) 421–429, https://doi.org/10.1016/j.nanoen.2018.03.062.

[9] X. Wang, Z. Wen, H. Guo, C. Wu, X. He, L. Lin, X. Cao, Z.L. Wang, Fully packaged blue energy harvester by hybridizing a rolling triboelectric nanogenerator and an electromagnetic generator, ACS Nano 10 (2016) 11369–11376, https://doi.org/10.1021/acsnano.6b06622.

[10] J. Wang, L. Geng, L. Ding, H. Zhu, D. Yurchenko, The state-of-the-art review on energy harvesting from flow-induced vibrations, Appl. Energy 267 (2020) 114902, https://doi.org/10.1016/j.apenergy.2020.114902.

[11] M. Shelley, N. Vandenberghe, J. Zhang, Heavy flags undergo spontaneous oscillations in flowing water, Phys. Rev. Lett. 94 (2005), 094302, https://doi.org/10.1103/PhysRevLett.94.094302.

[12] J.J. Allen, A.J. Smits, Energy harvesting EEL, J. Fluid. Struct. 15 (2001) 629–640, https://doi.org/10.1006/jfls.2000.0355.

[13] George W. Taylor, Joseph R. Burns, Sean M. Kammann, William B. Powers, T. R. Welsh, The energy harvesting EEL: a small subsurface ocean/river power generator, IEEE J. Ocean Eng. 26 (2001) 539–547, https://doi.org/10.1109/48.972090.

[14] A. Techet, J.J. Allen, A. Smits, Piezoelectric eels for energy harvesting in the ocean, in: Proceedings of the Twelfth (2002) International Offshore and Polar Engineering Conferenc, The International Society of Offshore and Polar Engineers, Kitakyushu, Japan.

[15] Y. Wang, J. Wang, X. Xiao, S. Wang, T.K. Phan, J. Dong, J. Mi, X. Pan, H. Wang, M. Xu, MALAT1 overexpression promotes the growth of colon cancer by repressing β-catenin degradation, Cell. Signal. 73 (2020), 109676, https://doi.org/10.1016/j.nanoen.2020.104736.

[16] P. Chen, J. An, S. Shu, R. Cheng, J. Nie, T. Jiang, Z.L. Wang, Super-durable, low-wear, and high-performance fur-brush triboelectric nanogenerator for wind and water energy harvesting for smart agriculture, Adv. Energy Mater. 11 (2021), 2003066, https://doi.org/10.1002/aenm.202003066.

[17] M. Xu, Y. Wang, S.L. Zhang, W. Ding, J. Cheng, X. He, P. Zhang, Z. Wang, X. Pan, Z. L. Wang, An aeroelastic flutter based triboelectric nanogenerator as a self-powered active wind speed sensor in harsh environment, Extrem. Mech. Lett. 15 (2017) 122–129, https://doi.org/10.1016/j.eml.2017.07.005.

[18] Y. Yang, G. Zhu, H. Zhang, J. Chen, X. Zhong, Z.-H. Lin, Y. Su, P. Bai, X. Wen, Z. L. Wang, Triboelectric nanogenerator for harvesting wind energy and as self-powered wind vector sensor system, ACS Nano 7 (2013) 9461–9468, https://doi.org/10.1021/nn4043157.

[19] H. Guo, X. He, J. Zhong, Q. Zhong, Q. Leng, C. Hu, J. Chen, L. Tian, Y. Xi, J. Zhou, A nanogenerator for harvesting airflow energy and light energy, J. Mater. Chem. A 2 (2014) 2079–2087, https://doi.org/10.1039/c3ta14421f.

[20] J. Hu, X. Pu, H. Yang, Q. Zeng, Q. Tang, D. Zhang, C. Hu, Y. Xi, A flutter-effect-based triboelectric nanogenerator for breeze energy collection from arbitrary directions and self-powered wind speed sensor, Nano Res. 12 (2019) 3018–3023, https://doi.org/10.1007/s12274-019-2545-y.

[21] Y. Su, Y. Yang, X. Zhong, H. Zhang, Z. Wu, Y. Jiang, Z.L. Wang, Fully enclosed cylindrical single-electrode-based triboelectric nanogenerator, ACS Appl. Mater. Interfaces 6 (2014) 553–559, https://doi.org/10.1021/am404611h.

[22] W. Zhong, L. Xu, H. Wang, D. Li, Z.L. Wang, Stacked pendulum-structured triboelectric nanogenerators for effectively harvesting low-frequency water wave energy, Nano Energy 66 (2019), 104108, https://doi.org/10.1016/j.nanoen.2019.104108.

[23] T.X. Xiao, T. Jiang, J.X. Zhu, X. Liang, L. Xu, J.J. Shao, C.L. Zhang, J. Wang, Z. L. Wang, Silicone-based triboelectric nanogenerator for water wave energy harvesting, ACS Appl. Mater. Interfaces 10 (2018) 3616–3623, https://doi.org/10.1021/acsami.7b17239.

[24] M. Xu, T. Zhao, C. Wang, S.L. Zhang, Z. Li, X. Pan, Z.L. Wang, High power density tower-like triboelectric nanogenerator for harvesting arbitrary directional water wave energy, ACS Nano 13 (2019) 1932–1939, https://doi.org/10.1021/acsnano.8b08274.

[25] X. Li, J. Tao, X. Wang, J. Zhu, C. Pan, Z.L. Wang, Networks of high performance triboelectric nanogenerators based on liquid-solid interface contact electrification for harvesting low-frequency blue energy, Adv. Energy Mater. 8 (2018), 1800705, https://doi.org/10.1002/aenm.201800705.

[26] C. Zhang, Y. Liu, B. Zhang, O. Yang, W. Yuan, L. He, X. Wei, J. Wang, Z.L. Wang, Harvesting wind energy by a triboelectric nanogenerator for an intelligent high-speed train system, ACS Energy Lett. 6 (2021) 1490–1499, https://doi.org/10.1021/acsenergylett.1c00368.

[27] Y. Xi, J. Wang, Y. Zi, X. Li, C. Han, X. Cao, C. Hu, Z. Wang, High efficient harvesting of underwater ultrasonic wave energy by triboelectric nanogenerator, Nano Energy 38 (2017) 101–108, https://doi.org/10.1016/j.nanoen.2017.04.053.

[28] L. Feng, G. Liu, H. Guo, Q. Tang, X. Pu, J. Chen, X. Wang, Y. Xi, C. Hu, Hybridized nanogenerator based on honeycomb-like three electrodes for efficient ocean wave energy harvesting, Nano Energy 47 (2018) 217–223, https://doi.org/10.1016/j.nanoen.2018.02.042.

[29] G. Liu, H. Guo, S. Xu, C. Hu, Z.L. Wang, Oblate spheroidal triboelectric nanogenerator for all-weather blue energy harvesting, Adv. Energy Mater. 26 (2019), 1900801, https://doi.org/10.1002/aenm.201900801.

[30] Z. Lin, B. Zhang, H. Guo, Z. Wu, H. Zou, J. Yang, Z.L. Wang, Super-robust and frequency-multiplied triboelectric nanogenerator for efficient harvesting water and wind energy, Nano Energy 64 (2019), 103908, https://doi.org/10.1016/j.nanoen.2019.103908.

[31] M. Xu, P. Wang, Y. Wang, S.L. Zhang, A.C. Wang, C. Zhang, Z. Wang, X. Pan, Z. L. Wang, A soft and robust spring based triboelectric nanogenerator for harvesting arbitrary directional vibration energy and self-powered vibration sensing, Adv. Energy Mater. 8 (2018), 1702432, https://doi.org/10.1002/aenm.201702432.

[32] X. Xiao, X. Zhang, S. Wang, H. Ouyang, P. Chen, L. Song, H. Yuan, Y. Ji, P. Wang, Z. Li, M. Xu, Z.L. Wang, Honeycomb structure inspired triboelectric nanogenerator for highly effective vibration energy harvesting and self-powered engine condition monitoring, Adv. Energy Mater. 9 (2019), 1902460, https://doi.org/10.1002/aenm.201902460.

[33] T. Du, X. Zuo, F. Dong, S. Li, A.E. Mtui, Y. Zou, P. Zhang, J. Zhao, Y. Zhang, P. Sun, M. Xu, A self-powered and highly accurate vibration sensor based on bouncing-ball triboelectric nanogenerator for intelligent ship machinery monitoring, Micromachines 12 (2021) 218, https://doi.org/10.3390/mi12020218.

[34] G. Liu, J. Chen, Q. Tang, L. Feng, H. Yang, J. Li, Y. Xi, X. Wang, C. Hu, Wireless electric energy transmission through various isolated solid media based on triboelectric nanogenerator, Adv. Energy Mater. 8 (2018), 1703086, https://doi.org/10.1002/aenm.201703086.

[35] T. Quan, Y. Wu, Y. Yang, Hybrid electromagnetic–triboelectric nanogenerator for harvesting vibration energy, Nano Res. 8 (2015) 3272–3280, https://doi.org/10.1007/s12274-015-0827-6.

[36] T. Quan, Y. Yang, Fully enclosed hybrid electromagnetic–triboelectric nanogenerator to scavenge vibrational energy, Nano Res. 9 (2016) 2226–2233, https://doi.org/10.1007/s12274-016-1109-7.

[37] H. Guo, Q. Leng, X. He, M. Wang, J. Chen, C. Hu, Y. Xi, A triboelectric generator based on checker-like interdigital electrodes with a sandwiched PET thin film for harvesting sliding energy in all directions, Adv. Energy Mater. 5 (2015), 1400790, https://doi.org/10.1002/aenm.201400790.

[38] Y. Yang, H. Zhang, Z.L. Wang, Direct-current triboelectric generator, Adv. Funct. Mater. 24 (2014) 3745–3750, https://doi.org/10.1002/adfm.201304295.

[39] T. Quan, Z.L. Wang, Y. Yang, A shared-electrode-based hybridized electromagnetic-triboelectric nanogenerator, ACS Appl. Mater. Interfaces 8 (2016) 19573–19578, https://doi.org/10.1021/acsami.6b07162.

[40] H. Zhao, X. Xiao, P. Xu, T. Zhao, L. Song, X. Pan, J. Mi, M. Xu, Z.L. Wang, TCF12 promotes the tumorigenesis and metastasis of hepatocellular carcinoma via upregulation of CXCR4 expression, Theranostics 9 (2019) 5810–5827, https://doi.org/10.1002/aenm.201902824.

[41] J. Yang, J. Chen, Y. Liu, W. Yang, Y. Su, Z.L. Wang, Triboelectrification-based organic film nanogenerator for acoustic energy harvesting and self-powered active acoustic sensing, ACS Nano 8 (2014) 2649–2657, https://doi.org/10.1021/nn4063616.

[42] B. Zhang, Z. Wu, Z. Lin, H. Guo, F. Chun, W. Yang, Z.L. Wang, All-in-one 3D acceleration sensor based on coded liquid–metal triboelectric nanogenerator for vehicle restraint system, Mater. Today 43 (2021) 37–44, https://doi.org/10.1016/j.mattod.2020.10.031.

[43] H. Wang, Z. Xiang, P. Giorgia, X. Mu, Y. Yang, Z.L. Wang, C. Lee, Triboelectric liquid volume sensor for self-powered lab-on-chip applications, Nano Energy 23 (2016) 80–88, https://doi.org/10.1016/j.nanoen.2016.02.054.

[44] X. Liu, K. Zhao, Z.L. Wang, Y. Yang, Unity convoluted design of solid Li-ion battery and triboelectric nanogenerator for self-powered wearable electronics, Adv. Energy Mater. 7 (2017), 1701629, https://doi.org/10.1002/aenm.201701629.

[45] B. Chen, N. Yang, Q. Jiang, W. Chen, Y. Yang, Transparent triboelectric nanogenerator-induced high voltage pulsed electric field for a self-powered handheld printer, Nano Energy 44 (2018) 468–475, https://doi.org/10.1016/j.nanoen.2017.12.026.

[46] X. Zhao, B. Chen, G. Wei, J.M. Wu, W. Han, Y. Yang, Polyimide/graphene nanocomposite foam-based wind-driven triboelectric nanogenerator for self-powered pressure sensor, Adv. Mater. Technol. 4 (2019), 1800723, https://doi.org/10.1002/admt.201800723.

[47] D.Y. Kim, H.S. Kim, D.S. Kong, M. Choi, H.B. Kim, J.-H. Lee, G. Murillo, M. Lee, S. S. Kim, J.H. Jung, Floating Buoy-based triboelectric nanogenerator for an effective

vibrational energy harvesting from irregular and random water waves in wild sea, Nano Energy 45 (2018) 247–254, https://doi.org/10.1016/j.nanoen.2017.12.052.

[48] Y. Xi, H. Guo, Y. Zi, X. Li, J. Wang, J. Deng, S. Li, C. Hu, X. Cao, Z.L. Wang, Multifunctional TENG for blue energy scavenging and self-powered wind-speed sensor, Adv. Energy Mater. 7 (2017), 1602397, https://doi.org/10.1002/aenm.201602397.

[49] L. Xu, T. Jiang, P. Lin, J.J. Shao, C. He, W. Zhong, X.Y. Chen, Z.L. Wang, Coupled triboelectric nanogenerator networks for efficient water wave energy harvesting, ACS Nano 12 (2018) 1849–1858, https://doi.org/10.1021/acsnano.7b08674.

[50] Gang Cheng, L. Zong-Hong, D. Zu-Liang, W. Zhong Lin, Simultaneously harvesting lectrostatic and mechanical energies from flowing water by a hybridized triboelectric nanogenerator, ACS Nano 8 (2013) 1932–1939, https://doi.org/10.1021/nn406565k.

[51] T. Kim, D.Y. Kim, J. Yun, B. Kim, S.H. Lee, D. Kim, S. Lee, Direct-current triboelectric nanogenerator via water electrification and phase control, Nano Energy 52 (2018) 95–104, https://doi.org/10.1016/j.nanoen.2018.07.048.

[52] Z. Zhao, X. Pu, C. Du, L. Li, C. Jiang, W. Hu, Z.L. Wang, Freestanding flag-type triboelectric nanogenerator for harvesting high-altitude wind energy from arbitrary directions, ACS Nano 10 (2016) 1780–1787, https://doi.org/10.1021/acsnano.5b07157.

[53] C. Ye, K. Dong, J. An, J. Yi, X. Peng, C. Ning, Z.L. Wang, A triboelectric–electromagnetic hybrid nanogenerator with broadband working range for wind energy harvesting and a self-powered wind speed sensor, ACS Energy Lett. 6 (2021) 1443–1452, https://doi.org/10.1021/acsenergylett.1c00244.

[54] Y. Wang, E. Yang, T. Chen, J. Wang, Z. Hu, J. Mi, X. Pan, M. Xu, A novel humidity resisting and wind direction adapting flag-type triboelectric nanogenerator for wind energy harvesting and speed sensing, Nano Energy 78 (2020), 105279, https://doi.org/10.1016/j.nanoen.2020.105279.

[55] Y. Bian, T. Jiang, T. Xiao, W. Gong, X. Cao, Z. Wang, Z.L. Wang, Triboelectric nanogenerator tree for harvesting wind energy and illuminating in subway tunnel, Adv. Mater. Technol. 3 (2018), 1700317, https://doi.org/10.1002/admt.201700317.

[56] M. Perez, S. Boisseau, P. Gasnier, J. Willemin, J.L. Reboud, An electret-based aeroelastic flutter energy harvester, Smart Mater. Struct. 24 (2015), 035004, https://doi.org/10.1088/0964-1726/24/3/035004.

[57] H. Phan, D. Shin, H. Sang, Y. Tae, P. Han, G. Kim, H. Kim, K. Kim, Y. Hwang, S. Hong, Aerodynamic and aeroelastic flutters driven triboelectric nanogenerators for harvesting broadband airflow energy, Nano Energy 33 (2017) 476–484, https://doi.org/10.1016/j.nanoen.2017.02.005.

[58] W. Sun, Z. Ding, Z. Qin, F. Chu, Q. Han, Wind energy harvesting based on fluttering double-flag type triboelectric nanogenerators, Nano Energy 70 (2020), 104526, https://doi.org/10.1016/j.nanoen.2020.104526.

[59] S. Niu, Y. Liu, X. Chen, S. Wang, Y.S. Zhou, L. Lin, Y. Xie, Z.L. Wang, Theory of freestanding triboelectric-layer-based nanogenerators, Nano Energy 12 (2015) 760–774, https://doi.org/10.1016/j.nanoen.2015.01.013.

[60] L. Zhu, C.S. Peskin, Simulation of a flapping flexible filament in a flowing soap film by the immersed boundary method, J. Comput. Phys. 179 (2002) 452–468, https://doi.org/10.1006/jcph.2002.7066.

[61] C. Eloy, C. Souilliez, L. Schouveiler, Flutter of a rectangular plate, J. Fluid. Struct. 23 (2007) 904–919, https://doi.org/10.1016/j.jfluidstructs.2007.02.002.

[62] C. Eloy, R. Lagrange, C. Souilliez, L. Schouveiler, Aeroelastic instability of cantilevered flexible plates in uniform flow, J. Fluid. Struct. 611 (2008) 97–106, https://doi.org/10.1017/S002211200800284X.

[63] O. Doaré, M. Sauzade, C. Eloy, Flutter of an elastic plate in a channel flow: confinement and finite-size effects, J. Fluid. Struct. 27 (2011) 76–88, https://doi.org/10.1016/j.jfluidstructs.2010.09.002.

[64] S. Michelin, S.G. Llewellyn Smith, B.J. Glover, Vortex shedding model of a flapping flag, J. Fluid Mech. 617 (2008) 1–10, https://doi.org/10.1017/s0022112008004321.

[65] E. Virot, X. Amandolese, P. Hémon, Fluttering flags: an experimental study of fluid forces, J. Fluid. Struct. 43 (2013) 385–401, https://doi.org/10.1016/j.jfluidstructs.2013.09.012.

[66] J.M. McCarthy, S. Watkins, A. Deivasigamani, S.J. John, Fluttering energy harvesters in the wind: a review, J. Sound Vibr. 361 (2016) 355–377, https://doi.org/10.1016/j.jsv.2015.09.043.

[67] D. Kim, J. Cossé, C. Huertas Cerdeira, M. Gharib, Flapping dynamics of an inverted flag, J. Fluid Mech. 736 (2013) R1, https://doi.org/10.1017/jfm.2013.555.

[68] U. Latif, E. Uddin, M.Y. Younis, J. Aslam, Z. Ali, M. Sajid, A. Abdelkefi, Experimental electro-hydrodynamic investigation of flag-based energy harvesting in the wake of inverted C-shape cylinder, Energy 215 (2021), 119195, https://doi.org/10.1016/j.energy.2020.119195.

[69] R. Song, X. Shan, F. Lv, T. Xie, A study of vortex-induced energy harvesting from water using PZT piezoelectric cantilever with cylindrical extension, Ceram. Int. 41 (2015) S768–S773, https://doi.org/10.1016/j.ceramint.2015.03.262.

[70] D.-A. Wang, D.-A. Wang, C.-W. Chao, J.M. Chen, A piezoelectric energy harvester based on pressure fluctuations in Kármán Vortex Street, in: Proceedings of the World Renewable Energy Congress-Sweden, Linköping University Electronic Press, Linköping, Sweden, pp. 1456–63.

[71] D.J. Olinger, Y. Wang, Hydrokinetic energy harvesting using tethered undersea kites, J. Renew. Sustain. Energy 7 (2015), 043114, https://doi.org/10.1063/1.4926769.

[72] R. Moodley, M. Nthontho, S. Chowdhury, S.P. Chowdhury, A technical and economic analysis of energy extraction from the Agulhas current on the east coast of South Africa, in: Proceedings of the 2012 IEEE Power and Energy Society General Meeting, IEEE, San Diego, CA, USA, pp. 1–8.

[73] M. Argentina, L. Mahadevan, Fluid-flow-induced flutter of a flag, Proc. Natl. Acad. Sci. USA 102 (2004) 1829–1834, https://doi.org/10.1073/pnas.0408383102.

[74] X. Shan, R. Song, B. Liu, T. Xie, Novel energy harvesting: a macro fiber composite piezoelectric energy harvester in the water vortex, Ceram. Int. 41 (2015) S763–S767, https://doi.org/10.1016/j.ceramint.2015.03.219.

[75] S. Alben, M.J. Shelley, Flapping states of a flag in an inviscid fluid: bistability and the transition to chaos, Phys. Rev. Lett. 100 (2008), 074301, https://doi.org/10.1103/PhysRevLett.100.074301.

[76] B.S.H. Connell, D.K.P. Yue, Flapping dynamics of a flag in a uniform stream, J. Fluid Mech. 581 (2007) 33–67, https://doi.org/10.1017/s0022112007005307.

[77] M.J. Shelley, J. Zhang, Flapping and bending bodies interacting with fluid flows, Annu. Rev. Fluid. Mech. 43 (2011) 449–465, https://doi.org/10.1146/annurev-fluid-121108-145456.

Yan Wang is currently pursuing his doctor degree in Dalian Maritime University, China. He is now a visiting PhD. Student of Professor Chengkuo Lee's group at National University of Singapore. His current research interests include flow-induced vibration, blue energy, self-powered system and triboelectric nanogenerator.

Xiangyu Liu is currently pursuing the master's degree in Dalian Maritime University, China. His current research interests in the self-powered system, blue energy and triboelectric nanogenerators.

Tianyu Chen is currently pursuing the master's degree in Dalian Maritime University, China His current research interests include flow-induced vibration, wind energy harvesting and triboelectric nanogenerator.

Hao Wang received his Ph.D. degree from Texas A&M University. Now he is an associate professor in Marine engineering College, Dalian Maritime University. His research interests include motion simulation, improvement, and stability analysis of the wave energy harvester.

Chuanqing Zhu is currently pursuing his doctor degree in Dalian Maritime University, China. His current research interests include blue energy, marine sensing, flow control and triboelectric nanogenerators.

Prof. Jianchun Mi received his Ph.D. degrees from Newcastle University in 1995. He was a national researcher and director researcher of Adelaide University in Australia from 1995 to 2006. He joined Peking University in 2006, and now he is a full professor in the College of Engineering. His research interests include turbulence, combustion and renewable energy.

Hongyong Yu is currently pursuing the master's degree in Dalian Maritime University, China. His current research interests in the triboelectric nanogenerators and blue energy

Prof. Chengkuo Lee received his Ph.D. degree in Precision engineering from The University of Tokyo in 1996. Currently, he is the director of Center for Intelligent Sensors and MEMS, and an Associate Professor in the Department of Electrical and Computer Engineering, National University of Singapore. In 2001, he cofounded Asia Pacific Microsystems, Inc., where he was the Vice President. From 2006 to 2009, he was a Senior Member of the Technical Staff at the Institute of Microelectronics, A-STAR, Singapore. He has contributed to more than 350 peer-reviewed international journal articles and 340 international conference papers and extended abstracts.

Liguo Song received his Ph.D. degree from Dalian Maritime University in 2020. He is a second engineer officer of ships powered by main propulsion machinery of 3000 kW propulsion power or more. Now he is an Associate Professor in the Marine Engineering College, Dalian Maritime University. His current research is mainly focused on the areas of blue energy, ship exhaust pollution control, triboelectric nanogenerators and its practical applications in smart ship and ocean.

Minyi Xu received his Ph.D. degree from Peking University in 2012. During 2016–2017, he joined Professor Zhong Lin Wang' group at Georgia Institute of Technology. Now he is a Professor in the Marine Engineering College, Dalian Maritime University. His current research is mainly focused on the areas of blue energy, self-powered systems, triboelectric nanogenerators and its practical applications in smart ship and ocean.

Pan Xinxiang received his B.E and Ph.D. degrees from Marine Engineering College, Dalian Maritime University, China, in 1987 and 1999. He now is President of Guangdong Ocean University. His research interests include smart and green ship, ocean engineering, energy saving and emission reduction, ship safety and pollution control, microfluidic chip, nano energy and self-powered systems.